water

MDPI

Article

Degradation of Tetracycline Using a Magnetic Gadolinium-Decorated Nanoplatform: A Peroxidase Biomimetic System with Fenton-Like Catalysis

Nesa Hamidian [1], Gholamreza Dehghan [1,*], Samaneh Rashtbari [1], Alireza Khataee [2,3,*], Mehdi Khoobi [4,5] and Nader Sheibani [6]

1 Department of Biology, Faculty of Natural Sciences, University of Tabriz, Tabriz 51666-16471, Iran
2 Research Laboratory of Advanced Water and Wastewater Treatment Processes, Department of Applied Chemistry, Faculty of Chemistry, University of Tabriz, Tabriz 51666-16471, Iran
3 Department of Environmental Engineering, Faculty of Engineering, Gebze Technical University, Gebze 41400, Turkey
4 Department of Radiopharmacy, Faculty of Pharmacy, Tehran University of Medical Sciences, Tehran 14176-14411, Iran
5 Biomaterials Group, Pharmaceutical Sciences Research Center, The Institute of Pharmaceutical Sciences (TIPS), Tehran University of Medical Sciences, Tehran 14176-14411, Iran
6 Department of Ophthalmology and Visual Sciences, Cell and Regenerative Biology, and Biomedical Engineering, University of Wisconsin School of Medicine and Public Health, Madison, WI 53705, USA
* Correspondence: gdehghan@tabrizu.ac.ir (G.D.); a_khataee@tabrizu.ac.ir or (A.K.)

Abstract: Pharmaceutical pollutants such as tetracycline (TC) pose a growing global threat to aquatic and terrestrial biodiversity. Developing new methods for the degradation of these pollutants would be a significant advancement in their management. The progress in the development of synthetic enzymes based on nanomaterials has resulted in their replacement for natural enzymes with higher performance quality. In this work, a magnetite/Gd^{3+}/β-cyclodextrin nanoplatform was prepared and used for TC degradation for the first time. The characterization studies were carried out using various methods, including SEM, XRD, and FTIR. The peroxidase-mimic activity of the synthesized nanoplatform was evaluated using a colorimetric assay. Kinetic parameters, including K_m and V_{max}, were obtained using TMB (3,3′,5,5′-tetramethylbenzidine) and H_2O_2. The results indicated that prepared particles had a lower K_m value than horseradish peroxidase (HRP), which confirmed the higher affinity of the prepared nanoplatform toward its substrates. We also demonstrated that our recyclable nanoplatform (3 mg/mL) was able to degrade 82% of TC (4.5 mM) in 85 min without any initiator such as light or ultrasonic waves. Collectively, these results confirmed the high affinity of the synthesized nanoplatform toward desired substrates, including TC.

Keywords: nanoplatform; tetracycline; peroxidase-mimic activity

Citation: Hamidian, N.; Dehghan, G.; Rashtbari, S.; Khataee, A.; Khoobi, M.; Sheibani, N. Degradation of Tetracycline Using a Magnetic Gadolinium-Decorated Nanoplatform: A Peroxidase Biomimetic System with Fenton-Like Catalysis. *Water* **2023**, *15*, 1419. https://doi.org/10.3390/w15071419

Academic Editor: Andrea G. Capodaglio

Received: 11 February 2023
Revised: 24 March 2023
Accepted: 1 April 2023
Published: 5 April 2023

1. Introduction

Recent studies suggest that tetracycline-like antibiotics rank second in manufacturing and utilization worldwide [1]. Tetracycline (TC) has been used since the 1950s for the treatment of gram-positive and gram-negative bacterial infections. It is also used to treat intracellular chlamydia, mycoplasmas, rickettsiae, protozoan parasites, and other non-infectious conditions [2]. In addition, this antibiotic has long been used in agriculture in North America as a growth stimulant for animals [3]. Other uses of this antibiotic include anti-inflammatory effects, suppression of the immune system, inhibition of lipase and collagenase activity, strengthening the binding of gingival fibroblasts, and wound healing [4]. Furthermore, TC is widely prescribed in veterinary medicine to remedy bacterial infections of the gastrointestinal tract, respiratory system, and skin, infections and

diseases of the musculoskeletal system, urinary tract, systemic infections, and sepsis [5]. In such cases, TC remains in animal products, including meat and milk, and is likely consumed by humans. TC can also enter the human body through direct or indirect means. The high rate of TC entrance into the body exacerbates gastrointestinal issues, allergies, liver damage, and antibiotic resistance [6]. Any reaction that can move TC from the states indicated for its antibacterial activity can be used as a means to destroy the structure of tetracycline. To ensure the degradation of this antibiotic, identification of its metabolites after degradation is essential.

Most conventional wastewater treatment plants are not designed to remove TC antibiotics from wastewater. In order to reduce the residues of this antibiotic in the environment, physicochemical methods, such as membrane filtration and adsorption using activated carbon, have been used [7]. However, the main drawback of such methods is that they do not remove the pollutants but transfer them from one phase to another. Today, advanced oxidation is proposed as an alternative method [8]. Less than 30% of the TC taken in through ingestion is metabolized, and the remainder enters the environment through human or animal excrement [9]. The best way to reduce and eliminate antibiotics, which come from unintended sources such as drinking water is through the use of degrading enzymes. These enzymes are mainly protein- and, to a lesser extent, RNA-structured. They are present in nature and living organisms, and they are important in research due to their high specificity and rapid reactions [10]. Enzymes can be used to break down TC. One of the most important enzymes that can break down TC is from the group of peroxidases, and studies show that TC in 50 g/L is degraded up to 72.5% by adding 40 U/L of manganese peroxidase. The rate of degradation depends on pH, temperature, and possibly H_2O_2 and manganese levels [11]. In recent years, we have seen an increase in mimicry in various fields of biology, chemistry, and other sciences. This science helps to develop suitable designs inspired by natural structures and mechanisms. Nanoscience is one of the most attractive fields of biomimetics [12,13]. However, natural enzymes have significant disadvantages, including low stability, high extraction costs, and a lower percentage of recovery, limiting thetheope of their application. To overcome these limitations and expand the utility of such enzymes, nanomaterials referred to as nanozymes are utilized for enzymatic activities [14–16].

The significant stability, ease of production, and recyclability of nanozymes provide conditions for their use as mimetic enzymes in biotechnology, laboratory diagnostics, and industry [17]. Given the advantages of nanozymes, in this study we prepared a nanozyme with peroxidase-like activity in place of peroxidase enzymes for TC degradation [18]. Nanozymes could successfully act as direct substitutes for natural enzymes for catalysis. With the rapid and better development of nanotechnology, nanozymes with higher catalytic activity, stability, and ease of modification and fabrication, compared with natural enzymes, are readily generated [19,20]. Their catalytic activity is shown to regulate the concentration of H_2O_2 in various microenvironments [21]. To save on the consumption of the catalyst, it can be recycled by different methods. Recovery methods include centrifugation, solvent evaporation, magnetic separation, and the use of pH against molecular and colloidal solvents [22]. The objective of this study was to design a nanoplatform with high catalytic power without the need for visible light, ultraviolet light, or an ultrasound, along with suitable recovery capability.

Peroxides are important natural enzymes in living organisms that break down hydrogen peroxide to produce hydroxyl radicals. Nanozymes that perform this action are included in peroxidase mimics. As in this study, some of these mimics are used to generate hydroxyl radicals [22]. The properties of peroxidase mimics are remarkable for their excellent substrate specificity and superior catalytic power. Unfortunately, low sensitivity, low operational stability, and high costs of catalyst preparation and purification limit their practicality; these properties must be improved [23,24].

The nanoplatform recovery feature is related to its magnetic properties. Magnetic properties are one of the attractive characteristics of nanoplatforms [25]. Lanthanide ions can exhibit strong magnetic properties due to their high spin number. This metal center

shows extensive variations in the spin quantum number and magnetic anisotropy [26]. A feature that makes this catalyst more attractive is the presence of cyclodextrin in the nanoplatform structure. Cyclodextrins are a group of cyclic oligosaccharides, including a macrocyclic ring that has 6 (α), 7 (β), and 8 (γ) glucopyranosyl subunits, which are linked by alpha-1-4 glycoside bonds [27]. Cyclodextrins are produced from starch by the glycosyltransferase enzymatic conversion. They are used in the food and pharmaceutical industries, as well as in chemical, agricultural, and environmental engineering [28]. Cyclodextrin has a hydrophilic surface with a lipophilic core, where molecules of suitable size can be stored to form non-covalent complexes, which results in an increase in water solubility and chemical stability [29]. The binding of guest molecules inside the host cyclodextrin is dynamic. The binding strength depends on how well the host-guest complexes fit together [30]. After assembling the nanoparticles and cyclodextrin, images and specifications of the desired nanoplatform are needed to ensure appropriate connections.

The purpose of using this coating along with iron nanoparticles is to create a good surface and increase the quality of the reaction. Experimental studies show that cyclodextrin increases the quality of the mentioned reactions [31,32]. Moreover, by applying changes such as connecting functional groups involved in catalysis, cyclodextrins can be given catalytic properties or they can be added to the catalyst as a speed increaser [32]. Cyclodextrin acts as a catalyst due to the presence of various functional groups; in addition to beta-cyclodextrin, it activates various organic compounds and increases the speed of reactions [33]. To identify and ensure antibiotic degradation analysis by spectroscopy, the method of studying absorption is utilized. Each substance has a separate absorbance peak, and after the reaction, it could decrease or increase. GC-mass spectroscopy is an analytical technique used to separate the chemical components of a sample mixture, and after detecting their presence or absence, one can determine their amounts [34]. Studies of catalysts show that some external factors increase the speed, quality, and catalytic power of some catalysts. A catalyst that works under the influence of an external source must first be stimulated by visible or ultraviolet lights or an ultrasound, and this energy should be decomposed into the pollutant [35]. A photocatalyst is a substance that absorbs light, raises that light's energy level, and gives that energy to the reactant so that a chemical reaction occurs. A heterogeneous photocatalyst is the most popular method for improving reaction performance [36]. In some research, nanozymes with photocatalytic properties have been utilized. In the reactions, first the solution is placed in a dark place, and then at certain time intervals, light is emitted and ultraviolet or visible light is irradiated. A photocatalyst that initiates catalysis under visible light has been used to remove water-polluting compounds such as phenol [37]. In other studies, ultrasound has been used to increase the quality of the reaction, which, like photocatalysis, starts the decomposition reaction and increases the decomposition power [37]. Nanozymes were used as enzymatic mimics to break down a variety of antibiotics, and adding nanozymes to the system with ultrasonic or visible light started and enhanced the degradation of antibiotics [38]. These studies showed that the removal efficiency of TC under natural sunlight conditions, without any catalyst, was 4.2% [39]. The efficiency of TC self-photolysis with visible light or sunlight simulation was less than 5% [40]. The presence of light enhanced the removal of TC by nanozymes [41]. In previous research, a photocatalyst and a sonocatalyst were used to remove an antibiotic from the group of tetracyclines, namely oxytetracycline [12].

Here a Fenton-like reaction method was used in this study. Fenton's reaction is a solution of hydrogen peroxide (H_2O_2) with a metal. Iron, copper, and manganese are the most common catalysts for Fenton-like reactions. Fe(II) attacks H_2O_2 in this reaction, producing powerful radical agents for decomposition [42]. Recently, advanced oxidation processes (AOPs) have been used for pollutant removal from wastewater because AOPs can oxidize a wide range of compounds. AOPs, using Fenton's reagent, have an effective degradation with low cost, non-toxicity of reagents, and a homogenous catalytic nature [43]. Magnetite (Fe_3O_4) has been studied to have especially powerful catalysis in a Fenton-like system, which is related to the presence of Fe(II) species in the magnetite structures that

started the Fenton reaction [44]. With an inverse spinel crystal structure, it shows unique electric and magnetic features based on the transfer of electrons between ferrous ions and ferric ions in the octahedral sites [45]. Experiments have proved that Fe_3O_4 nanoparticles can be heterogeneous Fenton-like, such as pH, the concentration of catalyst and H_2O_2, temperature, and pollutant concentration, which have been widely investigated because of their considerable effect on the removal of pollutants by the Fenton or Fenton-like process with in situ production of H_2O_2. Thus, all research should report the optimization of these parameters to increase the removal efficiency [46]. In the Fenton and electro-Fenton reactions, metal monoatomic catalysts (MSACs) are very useful for wastewater treatment due to the maximum atomic utilization of metal atoms, which have the advantages of homogeneous catalysts and heterogeneous catalysts; however, the content of monoatomic metals in MSACs is limited. Therefore, the development of bifunctional monoatomic catalysts for the high-efficiency production of H_2O_2 and •OH is highly desired but challenging. They also show poor stability, including resistance to acid corrosion and the ability to bind to supports [47]. Single-atom catalysts can reduce the loss of metal resources in the synthesis process and have excellent catalytic performance in the catalytic reaction process. By reducing the particle size from nanoclusters to the single atomic level, a strong increase in surface energy and 100% atomic utilization are guaranteed for their catalytic activity. Selective hydrogenation of unsaturated bonds (including carbon−carbon, nitro-gen−oxygen, carbon−oxygen, and carbon−nitrogen) affects the synthesis method, com-position content, monoatomic coordination, and charge relationship between metal and carrier and catalytic performance [48].

Fe-MOFs have strong coordination bonds, stable skeletons, Fe-O atoms, and narrow band gaps, as well as new porous inorganic-organic materials with multiple iron sites, which can make them excellent Fenton catalysts. Furthermore, the metal nodes of MOFs can be considered isolated semiconducting quantum dots that can be activated directly under light irradiation or with organic bonds as photoabsorbing antennas, turning Fe-MOFs into a more suitable photocatalyst in photo-Fenton systems. The synergistic effect of Fe−MOFs and photo−Fenton accelerates electron−hole separation and other catalysts such as Single−Atom Catalysts (SACs) with Peroxymonosulfate (PMS) systems are selective for types of organic pollutants removers, but their mechanisms remain ambiguous. Some research shows that radical oxidation (SO4•– and HO•) and the nonradical electron transfer pathway (ETP) coexist in the Co–N4–C/PMS system. Pollutants with a high redox potential were decomposed primarily by free radicals rather than ETP, while the oxidization of low-redox contaminants was dominated by ETP at the surface region of Co–N4–C, which overwhelmed the contributions of radicals in the homogeneous phase [49–51].

One of the improved methods of Fenton's method is the use of the electro-Fenton's method, in which an electric field is established that helps the production of radicals; the method is significantly improved, and the reaction efficiency increases [52]. In some studies, compared to AOS technology, O_3 has been used in the wastewater treatment process. Among the advantages of this method, it can be mentioned that it reacts quickly with bacteria, viruses, and protozoa, is effective in destroying organic substances and removing minerals, and is less affected by the pH. Specific conditions, and energy sources such as ultraviolet light are not needed. Although the ozonation process is a practical system, O_3 has low solubility and stability in water and a high production cost [53].

Compared to the previously mentioned methods, the catalyst used in this study does not require any external energy sources such as visible or UV light or electrodes. Moreover, the catalyst is recovered by an external magnet and reused. In addition, it is independent of H_2O_2.

2. Materials and Methods

2.1. Materials

Ferric chloride hexahydrate, ferrous chloride tetrahydrate, gadolinium (III) nitrate hexahydrate, β-cyclodextrin, diethylenetriaminepentaacetic acid (DTPA), acetic anhydride,

dimethyl sulfoxide (DMSO), triethylamine (Et3N), pyridine, hydrogen peroxide (H_2O_2, 30%), and sodium acetate were from Merck (Darmstadt, Germany), and acetic acid was from Sigma-Aldrich (St. Louis, MO, USA). The pure TC antibiotic was obtained from Kimia Pham Pharmaceutical Company (Tehran, Iran).

2.2. Synthesis of Nanoparticles

The synthesis of iron oxide nanoparticles with magnetic properties was performed by a co-precipitation method [47]. At first, 5.84 g of $FeCl_3$ and 2.15 g of $FeCl_2.4H_2O$ were dissolved in 100 mL of deionized (DI) water and stirred using a mechanical stirrer under nitrogen gas. In the next step, ammonium hydroxide (NH_4OH, 30 mL, 25%) was added to the prepared solution, and the mixture was stirred for another 1 h (1200 rpm) at 60 °C. The black precipitate produced was related to Fe_3O_4 NPs expelled by an external magnet and washed with water and ethanol several times. Finally, the produced product was dried under a vacuum at 60 °C for 12 h.

2.3. DTPA-DA Preparation

DTPA (0.125 moles), acetic anhydride (0.558 moles), and dry pyridine (0.770 moles) were mixed. The prepared mixture was then stirred at 65 °C for 24 h. The produced DTPA-DA was filtered, washed with diethyl ether, and dried under a vacuum [54].

2.4. Synthesis of PCD

For the synthesis of PCD, 1 mmol of anhydrous-CD was added to 4 mL of DMSO containing 1 mL of anhydrous Et_3N and stirred using magnetic stirring. During stirring, 8 mmol of DTPA-DA was added. The mixture was placed at 25 °C for 3 h to complete the polymerization reaction. The produced product was then washed with acetone, and the yellowish product was dried under a vacuum [55].

2.5. Coating of Fe_3O_4

Fe_3O_4 (2 g) was dispersed in 10 mL of DMSO in the first step. The βCD (1 mmol) and Et3 (1 mL) were added to the solution and stirred for 3 h. The prepared solution was stirred for an additional 3 h after adding DTPA-DA (8 mmol). Finally, the product was recovered with an external magnet, rinsed with ethanol, and dried under a vacuum for 1 day [56].

2.6. Loading of Gd^{3+} Ions to Fe_3O_4@PCD

Citrate buffer (0.1 M, pH = 5.5) (10 mL) was prepared, and Fe_3O_4@PCD (0.25 g) was dispersed in the buffer. The $Gd(NO_3)_3.6H_2O$ solution (0.35 g mL^{-1}) was added dropwise to the mixture. The prepared product was removed by an external magnet after being stirred at 100 °C for 24 h. It was then repeatedly rinsed with DI water and methanol before being dried under vacuum [57]. The added DTPA in the polymeric structure of PCD plays a crucial role in selective Gd^{3+} ion chelation by inhibiting Gd^{3+} leakage.

2.7. Characterization

The synthesized NPts were characterized using different methods, including FE-SEM (MIRA3 FEG-SEM, Tescan, Brno, Czech Republic), FT-IR, and XRD. The FT-IR spectra were obtained by an ALPHA II compact FT-IR spectrometer (Bruker, Bremen, Germany) in the range of 400–4000 cm^{-1}. X-ray (XRD) analysis was performed on an Empyrean-XRD Malvern Panalytical (Malvern, UK) in the range of 2θ = 10–70°. Furthermore, FE-SEM images were obtained using MIRA3TESCAN (Tescan, Brno, Czech Republic). The specific surface area of the prepared sample was measured using the Brunauer–Emmett–Teller (BET) analysis, which was carried out by N_2 adsorption and desorption isotherms at 77 K using the BELSORP (mini (II), Osaka, Japan).

2.8. Degradation of TC Using the Magnetite/Gd^{3+}/β-cyclodextrin Nanoplatform

Under the optimum conditions, 200 µL of TC (2 mg/mL) was dissolved in water containing 650 µL of catalysts with different concentrations (1 mg/mL, 2 mg/mL, or 3 mg/mL) and 150 µL of H_2O^2 (at 25 °C and pH 5). After the termination of the degradation reaction, the produced metabolites were analyzed by GC-MS spectroscopy (Agilent 6890N coupled with an Agilent 5973 mass spectrometer for GC-MS analysis, Agilent, Santa Clara, CA, USA).

3. Results

3.1. Characterization Studies

Figure 1 shows the FT-IR spectra of the prepared particles. The distinctive bands, which correspond to the stretching and bending vibrations of hydroxyl (OH) groups of β-cyclodextrin, were visible at 3390 and 1646 cm^{-1}, respectively [54]. The aliphatic C–H bond noted at 2800 cm^{-1} is related to the stretching bands at 1414 cm^{-1}. The observed peak at 1157 cm^{-1} could be associated with the stretching vibration of C–O–C bonds. Moreover, the C-OH stretching and vibration showed a band at 1031 cm^{-1} (Figure 2a) [54]. The peck of DTPA indicated that bands at 1732 and 1633 cm^{-1} could correspond to the stretching vibration of free monomer and carboxylate (–COO) in the carboxylic acid (COOH) groups [58]. The peaks at 1241 cm^{-1} and 1203 cm^{-1} corresponded to the stretching vibrations of C–O and C–N bonds, respectively (Figure 2b) [54]. The stretching vibration peaks of the asymmetric and symmetric carbonyl groups of DTPA-DA appear at 1821 cm^{-1} and 1775 cm^{-1}, respectively. Carboxylic acid groups led to a band at 1641 cm^{-1} of the spectrum (Figure 2c) [59]. Iron and oxygen bonds led to the formation of a sharp peak in the area of 586 cm^{-1}. In the PCD structure, the stretching and bending vibrations of O-H groups led to registered bands at 1631 and 1738 cm^{-1}, respectively (Figure 2d) [60]. A sharp peak at 576 cm^{-1} could be attributed to the Fe–O bonds of Fe_3O_4Npts. The bands at 3414 and 1618 cm^{-1} could be related to the stretching and bending vibrations of O-H groups, respectively (Figure 2e). Additionally, peaks at 1735 cm^{-1} are associated with ester carbonyl, and peaks at 1621 cm^{-1} correspond to carboxylate bonds (Figure 2f) [54]. In the free PCD spectrum, the bands were registered, and PCD-assembled Fe_3O_4 NPs displayed a band at approximately 580 cm^{-1}, verifying the correct organization of the polymer around the Fe_3O_4 NPs. The Fe_3O_4@PCD-Gd spectrum's band at 1737 cm^{-1} is related to the ester carbonyl that has been shifted to the lower frequencies [60]. The band was visible at 1568 cm^{-1} after Gd immobilization, which might be the result of the complexation of Gd^{+3} ions with PCD's carbonyl groups (Figure 2g,h) [61].

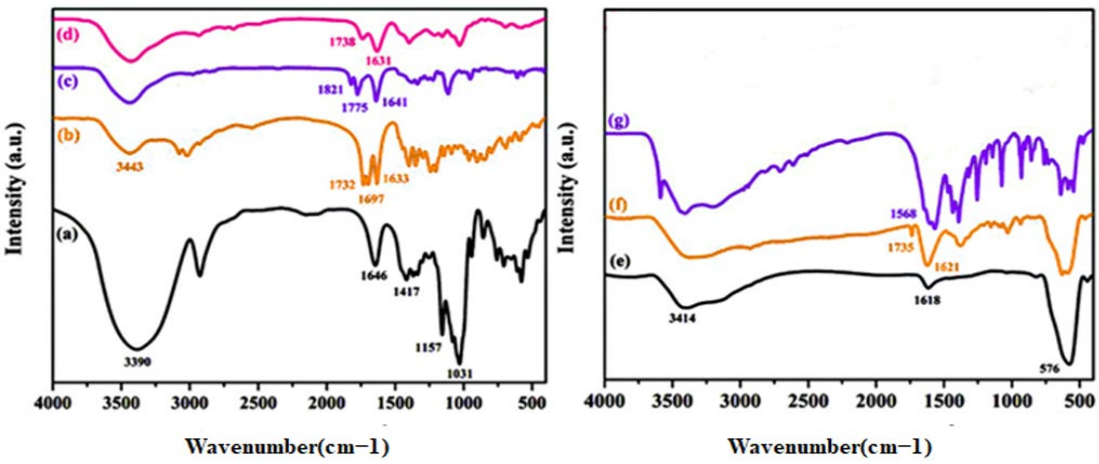

Figure 1. FTIR analysis of the synthesized magnetite/Gd^{3+}/β-cyclodextrin nanoplatform. FT-IR spectra of βCD (a), DTPA (b), DTPA-DA (c), PCD (d), Fe_3O_4 (e), Fe_3O_4@PCD (f), and Fe_3O_4@PCD-Gd (g).

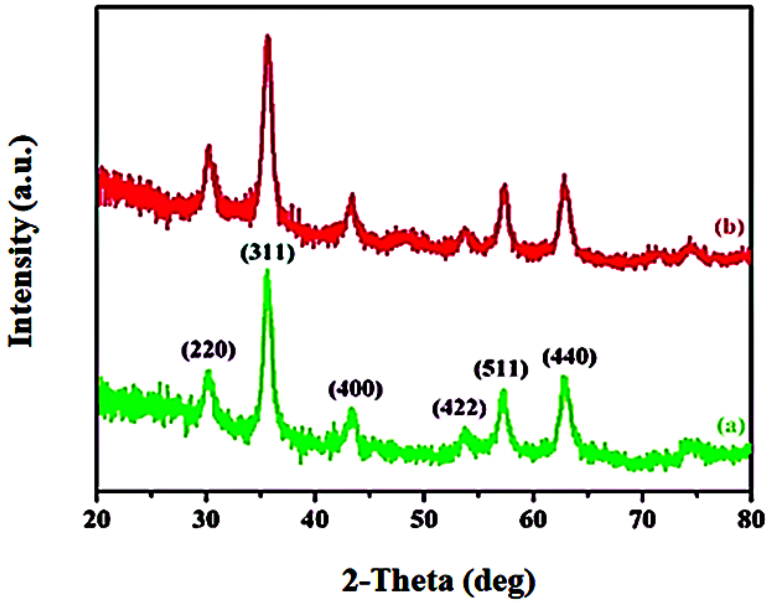

Figure 2. The XRD patterns of Fe_3O_4 (a) and Fe_3O_4@PCD-Gd (b) nanoparticles.

The XRD patterns of Fe_3O_4 and Fe_3O_4@PCD-Gd are presented in Figure 2. The observed characteristic peaks at 2θ = 30.35, 35.44, 42.82, 53.42, 57.16, 62.84, and 70 °C were consistent with the reflection values of the JCPDS card [62]. As shown in this figure, bands of Gd^{3+} ions were registered in the XRD patterns of Fe_3O_4@PCD-Gd. These outcomes demonstrated that the inverse spinel cubic structure of Fe_3O_4 NPs remained constant in the prepared samples and that ions were unable to alter the crystalline form of the Fe_3O_4 NPs [63]. The intensity was significantly decreased when compared to the data obtained from a data bank, indicating that the NPs components were successfully assembled.

Figure 3 shows the FE-SEM images of the synthesized Fe_3O_4@PCD-Gd NPs with different magnifications. According to these results, the prepared particles had a spherical shape and a uniform particle size distribution with a size of 57 nm [54].

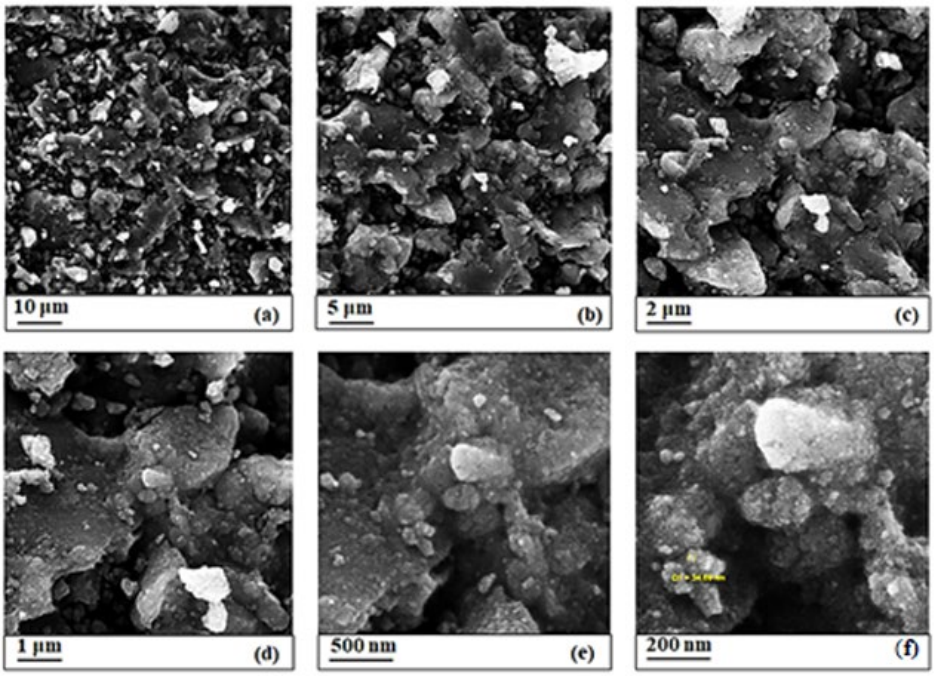

Figure 3. FE−SEM characterization of the synthesized magnetite/Gd^{3+}/β−cyclodextrin nanoplatform with different magnifications 10 µm (**a**), 5 µm (**b**), 2 µm (**c**), 1 µm (**d**), 500 nm (**e**), and 200 nm (**f**).

In addition, the elemental mapping and energy dispersive X-ray (EDX) spectrum of the sample are presented in Figure 4. As shown in this figure, it is clear that the synthesized NPs formed correctly, and the final product has three different elements, including Fe, O, C, and Gd.

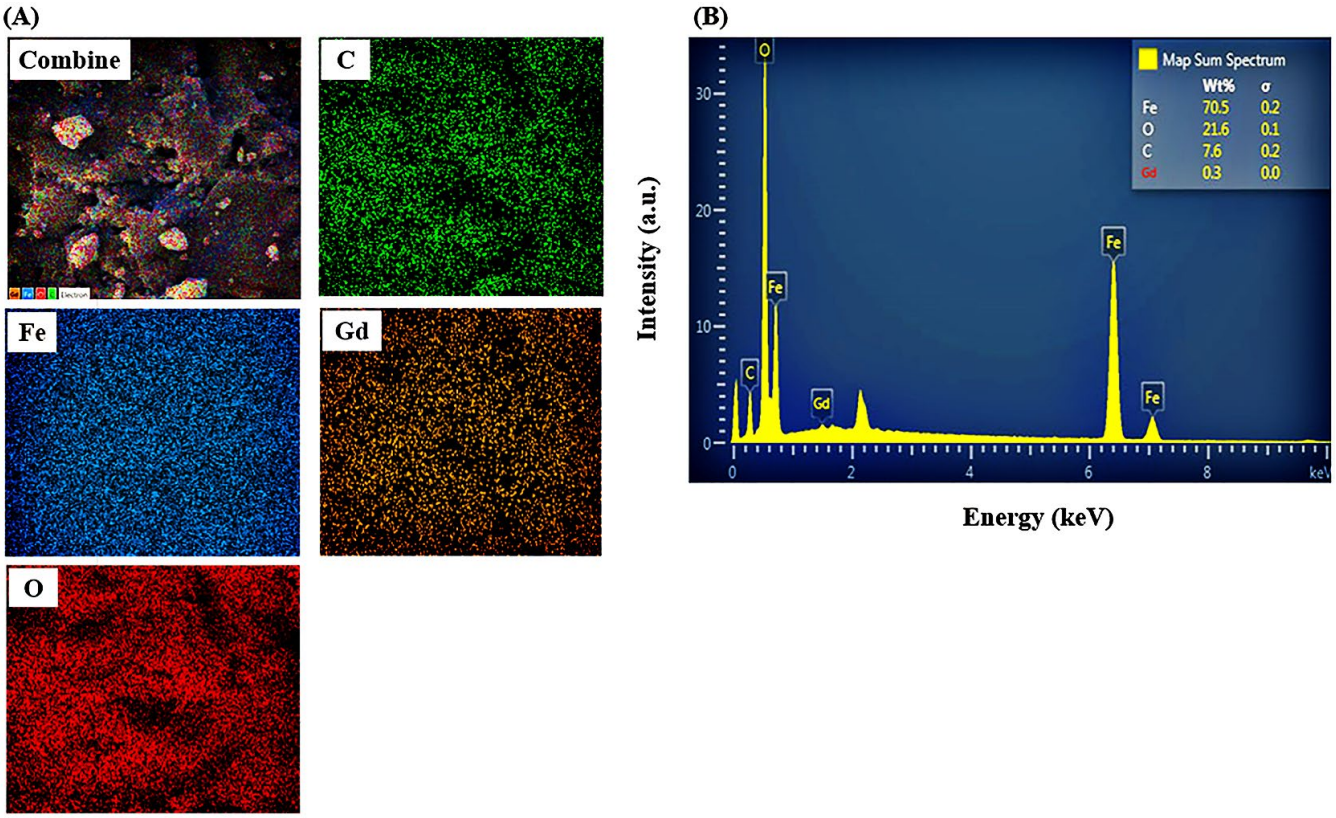

Figure 4. Elemental mapping (**A**) and EDAX (**B**) spectrum of the synthesized magnetite/Gd^{3+}/β-cyclodextrin nanoplatform.

The specific surface area of the synthesized magnetite/Gd^{3+}/β-cyclodextrin nanoplatform was evaluated by the BET method using the adsorption of nitrogen. The results are shown in Figure 5. According to the results, the mean surface area and the pore volume of the prepared particles were calculated as 56.12 m^2/g and 0.155 m^3/g, respectively. In addition, Figure 5A shows a classical IV isotherm type, suggesting the presence of a mesoporous structure [64]. The pore size distribution of the sample as estimated according to the BJH method from the adsorption branch is depicted in Figure 5B. It can be seen that the diameter range of pores was from 1.5 to 10 nm, and the mean diameter of pores is 3.1 nm.

3.2. Enzyme-Like Activity of the Nanoplatform

To identify the peroxidase-like activity of our nanoplatform, a colorimetric assay based on the oxidation of TMB was used. For this purpose, the oxidation of TMB in the presence of H_2O_2 was catalyzed by various concentrations of the nanoplatform, which resulted in the production of a bluish-green product. In the process of the reaction, a blue-colored product with a maximum absorbance at 652 nm was produced, along with the TMB cation free radical and a one-electron oxidation product. Additionally, control experiments were carried out under the same experimental condition to investigate the peroxidase-like activity of β-cyclodextrin. The results showed no peroxidase-mimic activity of the β-cyclodextrin. In combination with nanoplatforms, it increases the quality and power of the catalyst (Figure S1A).

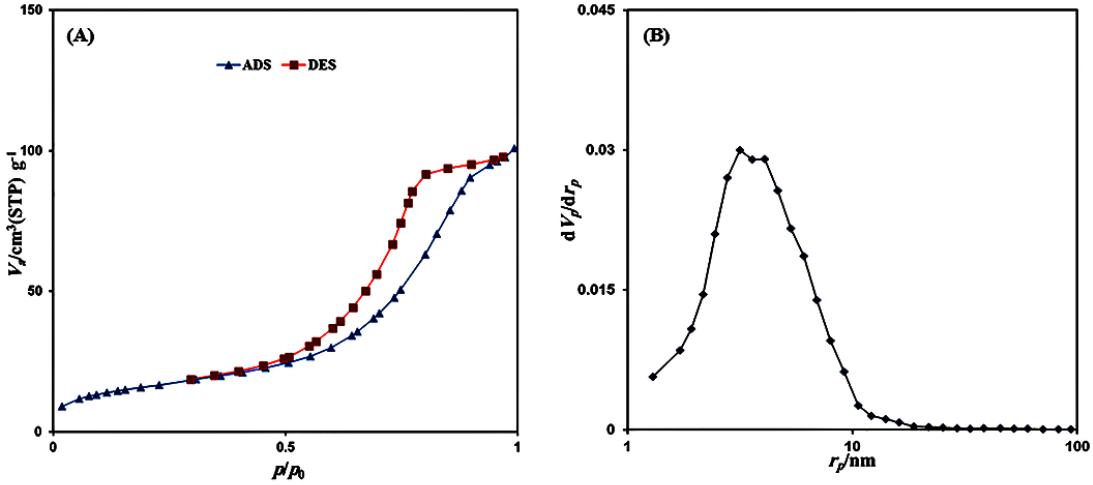

Figure 5. N_2 adsorption–desorption isotherms (**A**) and pore size distribution (**B**) of the synthesized nanoplatform in optimal conditions.

3.3. Hydroxyl Radical Scavengers

The formation of hydroxyl radicals (•OH) in the presence of the peroxidase-mimic nanoplatform was tested using the radical-scavenging activities of vitamin C, methanol, and ethanol. The absorption spectra of the prepared samples without and with different scavengers were recorded, and the results showed a significant decrease in the absorption spectra of the samples, indicating the presence of hydroxyl radicals (Figure S1B).

3.4. Optimization

At first, optimization of the experimental conditions for the enzyme-mimic activity of the prepared nanoplatform was performed. Experimental results indicated that the optimum temperature, pH, and catalyst concentration for the catalytic activity were 25 °C, 5.0, and 3 mg/mL, respectively (Figure 6).

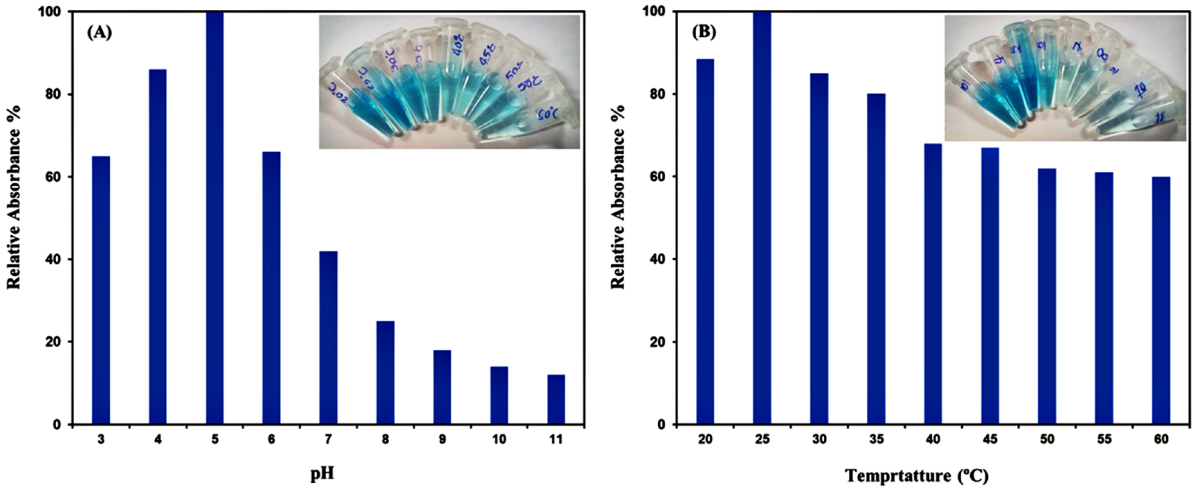

Figure 6. Effects of various pH (**A**) and temperatures (**B**) on the peroxidase-mimicking activity of the nanoplatform.

It has been reported that the optimum conditions result in the generation of small, highly crystalline, and monodispersed particles. Therefore, it can be expected that dispersion of the nanoplatform can occur entirely at pH 5.0 and 25 °C and that most particle surface active sites can be exposed to the substrate molecules. Furthermore, the generation of small particles could increase surface-to-volume ratios. Large surface area will lead to high catalytic activity. However, the catalytic activity of the prepared particles decreased

at higher pH and temperature due to the aggregation of the particles and the decreased surface-to-volume ratios (because of the increase in the particles' size) [14,15].

3.5. Kinetic Studies

The enzymatic activity of our nanoplatform was evaluated with TMB and H_2O_2 (as substrates) to adjust enzymatic properties. The kinetic parameters of the nanoplatform, in the presence or absence of H_2O_2, were then calculated [65]. In this regard, Michaelis–Menten and Lineweaver–Burk curves were plotted using additional concentrations of TMB and H_2O_2 (Figure S2).

The kinetic parameters, including V_{max} and K_m, were then calculated and are listed in Table 1. K_m showed the affinity between the enzyme and substrate. A low K_m indicates high affinity, and K_m comparisons indicate the kinetic parameters.

Table 1. Comparison of the calculated kinetic parameters (V_{max} and K_m) for the peroxidase-mimic magnetite/Gd^{3+}/β-cyclodextrin nanoplatform with HRP.

Sample	Substrate	K_m (mM)	V_{max} (M s^{-1})	Ref.
HRP	TMB	0.434	2.01×10^{-8}	[66]
	H_2O_2	3.7	3.34×10^{-8}	
Nanoplatform	TMB	0.5×10^{-4}	13.6×10^{-7}	This work
	H_2O_2	2.4×10^{-4}	17.8×10^{-8}	

3.6. Effect of the Nanoplatform Concentration on TC Degradation

Under optimal conditions, the degradation reaction was initiated, and after the completion of the reaction, the solution was analyzed using UV/Vis spectrophotometry. According to the spectrophotometric results, 82% of TC was degraded in 85 min. The percent degradation was constant (82%) at different catalyst concentrations (3 mg/mL, 2 mg/mL, or 1 mg/mL), but degradation time decreased with increasing the nanoplatform concentration (Figure 7A).

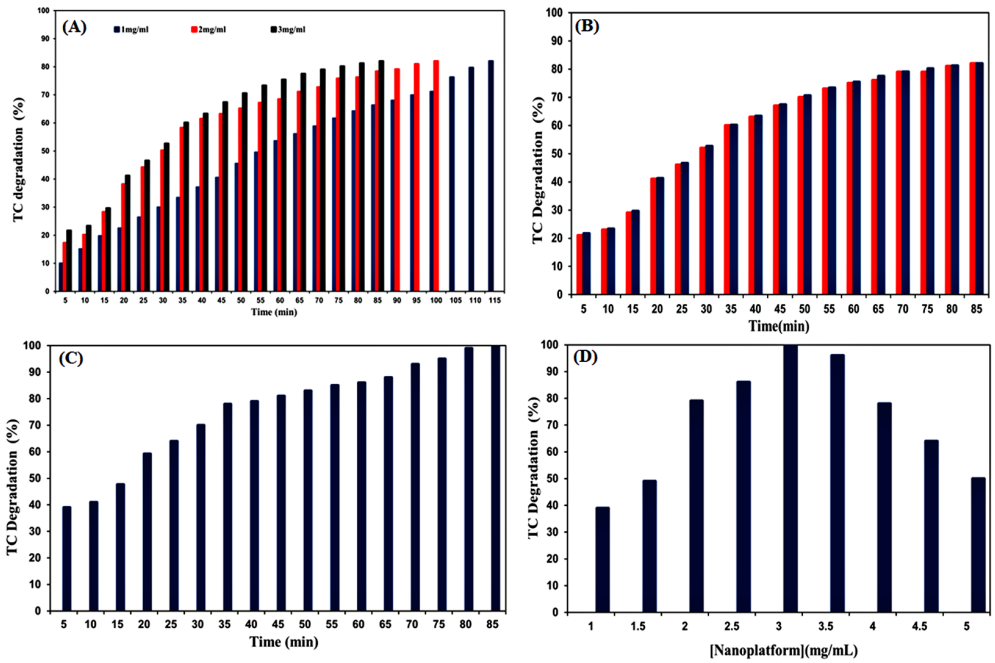

Figure 7. Effects of different concentrations of nanoplatform (**A**), H_2O_2 (**B**), incubation time (**C**), and the concentration of magnetite/Gd^{3+}/β-cyclodextrin nanoplatform (**D**) on the degradation of TC in the presence of H_2O_2.

3.7. The Effect of H_2O_2 Concentration on TC Degradation

Various concentrations of H_2O_2 were added to the reaction solution to study the impact of H_2O_2 concentration on TC degradation. In one degradation reaction, the ratio of 3 (distilled water) to 1 (H_2O_2) dilution was compared with the ratio of 1 to 1 dilution of water to H_2O_2. The obtained results revealed that there were no significant changes in the rate and percentage of TC degradation with increasing H_2O_2 concentration. Therefore, the degradation efficiency of TC was independent of H_2O_2 concentration (Figure 7B).

3.8. Recovery of the Nanoplatform

Using an external magnet, after the completion of the degradation process, the nanoplatform was recovered from the reaction solution and used in a new reaction. These results indicated that the catalyst was able to degrade 82% of TC in 122 min. Thus, the degradation time was increased in the second cycle (Figure 7C,D).

3.9. Performance of the Catalyst in the Presence of UV and Visible Light

The possible effect of UV and visible light on the degradation efficiency of TC was tested. The obtained results showed no significant effect of visible or UV light on the degradation of TC (Figure S3).

3.10. Proposed Pathway of TC Degradation

Various metabolites and their corresponding chemical structures were identified by matching their spectra with those recorded in the NIST 20 Mass Spectral Library. The intermediate products obtained from the degradation of TC included: TC (1), 4H-naphtho[1,2-b] pyran-4-one (2), naphthalene (3), bisabolol (4), and hexadecanoic acid (5). These were analyzed by GC–MS, confirming the proposed pathway of TC degradation using our nanoplatform (Figure 8). Figure S4 shows the GC-MS profile of degradation products of TC.

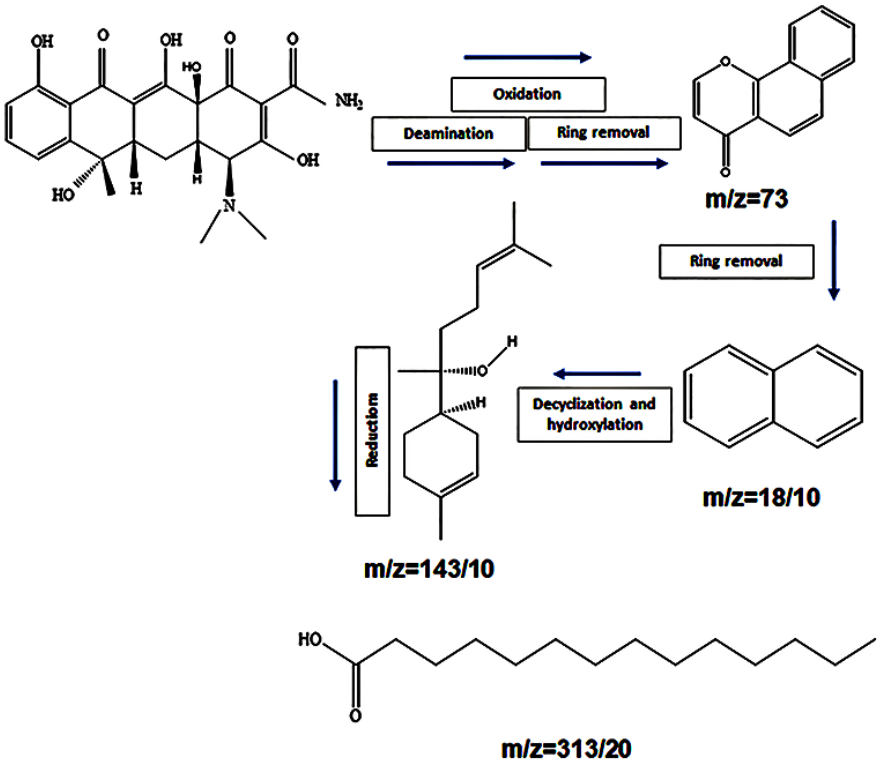

Figure 8. The proposed pathway for degradation of TC in the presence of the magnetite/Gd^{3+}/β-cyclodextrin nanoplatform.

3.11. Degradation Kinetic Analysis

TC degradation analysis was performed using the decrease in absorption of TC over a period of 5 min and the kinetic constant of degradation was calculated from the slope of the graph (Figure S5). The results indicated that the kinetic constant of TC degradation was 17×10^{-3} min^{-1}.

4. Discussion

Due to the existence of TC residuals in drinking water, their degradation is of significant importance to human health and the environment. Here TC was degraded by up to 82% using a novel nanozyme. At low catalyst concentrations, the TC degradation efficiency remained constant at 82%. Thus, preserving the amount of catalyst consumption is advantageous and makes TC removal cost-effective. To increase the rate of degradation, the concentration of the catalyst can be increased, which reduces the duration of the degradation. In previous studies visible and ultraviolet lights and ultrasound was used to increase the degradation percentage above 70%. In the method described here, other external factors such as ultraviolet light and ultrasound sources were not required [67]. Thus, the catalyst starts and continues the reaction, and for this reason, it is a simple and low-cost method. The presence of an artificial catalyst creates a secondary pollutant in the system, which in many methods is not removed from the system after the catalyst reaction has occurred. In the present study, the catalyst was removed from the system using the nanozyme's magnetic properties reducing its harmful effects on the environment and other biological systems. In addition, the catalyst retains the ability to decompose TC after recovery and could be used for additional analytical reactions. Thus, the nanoplatform developed here is economical.

Hydrogen peroxide, an additive that is used for peroxidation reactions, has not been reported to be harmful to the environment, aquatic animals, plants, or other species in low concentrations without changing its chemical structure. Hydrogen peroxide is also used by other organisms in the environment. It is produced as a result of metabolism, but excess hydrogen peroxide in the environment and its degradation into hydroxyl radicals can attack and destroy DNA or proteins with adverse effects [68]. The independence of the designed catalyst from hydrogen peroxide is another advantage, as it does not require the use of hydrogen peroxide in the environment to increase the speed and quality of the reaction.

The nanoplatform developed here showed that the majority of its activities were achieved at pH 5. Under laboratory conditions, this possibility is provided by the desired pH. However, under non-laboratory conditions, such as sewers and external environments, this is not possible. In the external environment, pH varies in the range of 3.5 to 6.5, which does not provide a suitable pH. Thus, the use of catalysts whose activity is pH independent is desirable and another noteworthy point in the studies presented here is that the metabolites resulting from TC degradation remain in the environment and cause pollution. Thus, the design of nanoplatforms with absorbent properties that can be removed makes these metabolites beneficial [69]. Nanoparticles that have high porosity and superior characteristics can remove the metabolites with high efficiency without catalysis [70]. Although this absorption is not 100% in most cases, it can significantly reduce the resultant metabolites created from TC degradation. Improving the efficiency of nanoplatforms with catalytic activities and without the least secondary damage to the environment requires comprehensive and detailed structural and enzyme studies. The current method has increased the percentage of degradation and reduced the required steps and tools, and catalyst recovery, thus making it cost-effective and timely with a significant improvement compared with previous methods.

5. Conclusions

The nanoplatform developed here, to the best of our knowledge, is the first with multiple desirable features. In addition to its recyclability, increased catalysis quality, and strengthening of the magnetic power of Fe_3O_4 nanoparticles, it mediates TC degradation without the need for external initiators such as light or ultrasound. It degrades TC up to 82% in 85 min at a temperature of 25 °C and pH 5. Compared to natural enzymes, this nanoplatform had lower K_m and higher V_m values (maximum rate) under normal conditions and at the same mass concentration. The pathway of degradation includes ring removal, deamination, and oxidation in the next steps of hydroxylation and reduction. The compounds produced included 4H-Naphtho[1,2-b]pyran-4-one, naphthalene, bisabolol, and hexadecanoic acid, which were identified by GC-mass spectrometry.

Supplementary Materials: The following supporting information can be downloaded at: https://www.mdpi.com/article/10.3390/w15071419/s1, Figure S1: Study of the peroxidase-like activity of only β-cyclodextrin and in the combination of nanoplatform (A) and the effect of radical scavengers on the produced •OH (B); Figure S2: Lineweaver–Burk curve for the peroxidase-mimicking activity of the synthesized nanoplatform in the presence of TMB (A) and H2O2 (B) as substrates; Figure S3: Effect of visible and UV light on the percentage of TC degradation; Figure S4: GC-MS profile of degradation products of TC; Figure S5: Degradation kinetic constant of TC.

Author Contributions: G.D., Conceptualization, project administration, writing—review and editing. N.H., Investigation, data curation, writing—original draft. S.R., Validation, analysis, and editing. N.S., Validation, review, and editing. A.K., Critical review, commentary, and review and editing. M.K., Provision of study materials. All authors have read and agreed to the published version of the manuscript.

Funding: This research received no external funding.

Data Availability Statement: Not applicable.

Acknowledgments: The authors thank the University of Tabriz for support.

Conflicts of Interest: The authors declare no conflict of interest.

References

1. Ahmad, F.; Zhu, D.; Sun, J. Environmental fate of tetracycline antibiotics: Degradation pathway mechanisms, challenges, and perspectives. *Environ. Sci. Eur.* **2021**, *33*, 64. [CrossRef]
2. Eliopoulos, G.M.; Eliopoulos, G.M.; Roberts, M.C. Tetracycline therapy: Update. *Clin. Infect. Dis.* **2003**, *36*, 462–467.
3. Bacanlı, M.; Başaran, N.J.F.; Toxicology, C. Importance of antibiotic residues in animal food. *Food Chem. Toxicol.* **2019**, *125*, 462–466. [CrossRef]
4. Yanamoto, S.; Soutome, S.; Tsuda, S.; Morishita, K.; Hayashida, S.; Harata, S.; Murata, M.; Omori, K.; Rokutanda, S.; Umeda, M. Inhibitory effect of topical antibiotics/antiseptics administration on bacterial growth in the open wound of the jawbone surgery: Randomized controlled, preliminary study. *J. Dent. Sci.* **2021**, *16*, 154–159. [CrossRef] [PubMed]
5. Prescott, J.F.; Baggot, J.D.; Walker, R.D. *Antimicrobial Therapy in Veterinary Medicine*; Iowa State University Press: Ames, IA, USA, 2000.
6. Faria, L.V.; Lima, A.P.; Araújo, F.M.; Lisboa, T.P.; Matos, M.A.; Munoz, R.A.; Matos, R.C. High-throughput amperometric determination of tetracycline residues in milk and quality control of pharmaceutical formulations: Flow-injection versus batch-injection analysis. *Anal. Methods* **2019**, *11*, 5328–5336. [CrossRef]
7. Al-Dhabi, N.A.; Esmail, G.A.; Arasu, M.V. Effective degradation of tetracycline by manganese peroxidase producing *Bacillus velezensis* strain Al-Dhabi 140 from Saudi Arabia using fibrous-bed reactor. *Chemosphere* **2021**, *268*, 128726. [CrossRef]
8. Vagi, M.C.; Petsas, A.S. Recent advances on the removal of priority organochlorine and organophosphorus biorecalcitrant pesticides defined by Directive 2013/39/EU from environmental matrices by using advanced oxidation processes: An overview (2007–2018). *J. Environ. Chem. Eng.* **2020**, *8*, 102940. [CrossRef]
9. Daghrir, R.; Drogui, P. Tetracycline antibiotics in the environment: A review. *Environ. Chem. Lett.* **2013**, *11*, 209–227. [CrossRef]
10. Copeland, R.A. *Enzymes: A Practical Introduction to Structure, Mechanism, and Data Analysis*; John Wiley & Sons: Hoboken, NJ, USA, 2023.
11. Wen, X.; Jia, Y.; Li, J. Enzymatic degradation of tetracycline and oxytetracycline by crude manganese peroxidase prepared from *Phanerochaete chrysosporium*. *J. Hazard. Mater.* **2010**, *177*, 924–928. [CrossRef]
12. Garg, P.; Ghatmale, P.; Tarwadi, K.; Chavan, S. Influence of nanotechnology and the role of nanostructures in biomimetic studies and their potential applications. *Biomimetics* **2017**, *2*, 7. [CrossRef]
13. Dehghan, G.; Rashtbari, S.; Yekta, R.; Sheibani, N. Synergistic inhibition of catalase activity by food colorants sunset yellow and curcumin: An experimental and MLSD simulation approach. *Chem. Biol. Interact.* **2019**, *311*, 108746.

14. Rashtbari, S.; Dehghan, G.; Amini, M. An ultrasensitive label-free colorimetric biosensor for the detection of glucose based on glucose oxidase-like activity of nanolayered manganese-calcium oxide. *Anal. Chim. Acta* **2020**, *1110*, 98–108. [CrossRef] [PubMed]
15. Rashtbari, S.; Dehghan, G.; Khataee, S.; Amini, M.; Khataee, A. Dual enzymes-mimic activity of nanolayered manganese-calcium oxide for fluorometric determination of metformin. *Chemosphere* **2022**, *291*, 133063. [CrossRef] [PubMed]
16. Suliman, M.H.; Yamani, Z.H.; Usman, M. Electrochemical Reduction of CO_2 to C1 and C2 Liquid Products on Copper-Decorated Nitrogen-Doped Carbon Nanosheets. *Nanomaterials* **2023**, *13*, 47. [CrossRef]
17. Gkantzou, E.; Chatzikonstantinou, A.V.; Fotiadou, R.; Giannakopoulou, A.; Patila, M.; Stamatis, H. Trends in the development of innovative nanobiocatalysts and their application in biocatalytic transformations. *Biotechnol. Adv.* **2021**, *51*, 107738. [CrossRef]
18. Tang, S.; Zhao, M.; Yuan, D.; Li, X.; Wang, Z.; Zhang, X.; Jiao, T.; Ke, J. Fe_3O_4 nanoparticles three-dimensional electro-peroxydisulfate for improving tetracycline degradation. *Chemosphere* **2021**, *268*, 129315. [CrossRef]
19. Rashtbari, S.; Dehghan, G.; Khorram, S.; Amini, M.; Khataee, A.; Yoon, Y. Plasma modified Co_3O_4 nanoparticles for catalytic degradation process through enhanced peroxidase-like activity. *J. Ind. Eng. Chem.* **2023**, *121*, 114–123. [CrossRef]
20. Rashtbari, S.; Dehghan, G. Biodegradation of malachite green by a novel laccase-mimicking multicopper BSA-Cu complex: Performance optimization, intermediates identification and artificial neural network modeling. *J. Hazard. Mater.* **2021**, *406*, 124340. [CrossRef]
21. Jiang, D.; Ni, D.; Rosenkrans, Z.T.; Huang, P.; Yan, X.; Cai, W. Nanozyme: New horizons for responsive biomedical applications. *Chem. Soc. Rev.* **2019**, *48*, 3683–3704. [CrossRef]
22. Thangudu, S.; Su, C.-H. Peroxidase mimetic nanozymes in cancer phototherapy: Progress and perspectives. *Biomolecules* **2021**, *11*, 1015. [CrossRef]
23. Thangudu, S.; Lee, M.T.; Rtimi, S. Tandem synthesis of high yield MoS_2 nanosheets and enzyme peroxidase mimicking properties. *Catalysts* **2020**, *10*, 1009. [CrossRef]
24. Thangudu, S.; Chiang, C.-S.; Hwang, K.C. 1550 nm light activatable photothermal therapy on multifunctional $CuBi_2O_4$ bimetallic particles for treating drug resistance bacteria-infected skin in the NIR-III biological window. *J. Colloid Interface Sci.* **2023**, *631*, 1–16. [CrossRef]
25. Bao, S.; Wang, Y.; Wei, Z.; Yang, W.; Yu, Y. Highly efficient recovery of heavy rare earth elements by using an amino-functionalized magnetic graphene oxide with acid and base resistance. *J. Hazard. Mater.* **2022**, *424*, 127370. [CrossRef] [PubMed]
26. Vieru, V.; Iwahara, N.; Ungur, L.; Chibotaru, L.F. Giant exchange interaction in mixed lanthanides. *Sci. Rep.* **2016**, *6*, 24046. [CrossRef] [PubMed]
27. Yu, Y.; Delbianco, M. Synthetic polysaccharides. In *Recent Trends in Carbohydrate Chemistry*; Elsevier: Amsterdam, The Netherlands, 2020; pp. 333–371.
28. Petitjean, M.; García-Zubiri, I.X.; Isasi, J.R. History of cyclodextrin-based polymers in food and pharmacy: A review. *Environ. Chem. Lett.* **2021**, *19*, 3465–3476. [CrossRef]
29. Kondiah, P.; Choonara, Y.E.; Hayiyana, Z.; Kondiah, P.J.; Marimuthu, T.; du Toit, L.C.; Kumar, P.; Pillay, V. Multi-Cyclodextrin Supramolecular Encapsulation Entities for Multifaceted Topical Drug Delivery Applications. In *Applications of Encapsulation and Controlled Release*; CRC Press: Boca Raton, FL, USA, 2019; pp. 1–17.
30. Khalili, L.; Dehghan, G.; Sheibani, N.; Khataee, A. Smart active-targeting of lipid-polymer hybrid nanoparticles for therapeutic applications: Recent advances and challenges. *Int. J. Biol. Macromol.* **2022**, *213*, 166–194. [CrossRef]
31. Muthukrishnan, L. Disruptive Nanozyme Technology for Futuristic Bio-Medical and Bio-imaging Applications. *Curr. Nanosci.* **2021**, *17*, 853–870. [CrossRef]
32. Dalal, D.S.; Patil, D.R.; Tayade, Y.A. β-Cyclodextrin: A Green and Efficient Supramolecular Catalyst for Organic Transformations. *Chem. Rec.* **2018**, *18*, 1560–1582. [CrossRef]
33. Fiorentin, T.R.; Logan, B.K.; Martin, D.M.; Browne, T.; Rieders, E.F. Assessment of a portable quadrupole-based gas chromatography mass spectrometry for seized drug analysis. *Forensic Sci. Int.* **2020**, *313*, 110342. [CrossRef]
34. Goh, P.S.; Samavati, Z.; Ismail, A.F.; Ng, B.C.; Abdullah, M.S.; Hilal, N. Modification of Liquid Separation Membranes Using Multidimensional Nanomaterials: Revealing the Roles of Dimension Based on Classical Titanium Dioxide. *Nanomaterials* **2023**, *13*, 448. [CrossRef]
35. Norabadi, E.; Jahantiq, A.; Kamani, H. Synthesis of Fe-TiO_2@Fe_3O_4 magnetic nanoparticles as a recyclable sonocatalyst for the degradation of 2, 4-dichlorophenol. *Environ. Sci. Pollut. Res.* **2022**, *30*, 31446–31460. [CrossRef] [PubMed]
36. Chen, J.; Xu, X.; Feng, L.; He, A.; Liu, L.; Li, X.; Khan, S.; Chen, Y. One-step MOF assisted synthesis of $SmVO_4$ nanorods for photocatalytic degradation of tetracycline under visible light. *Mater. Lett.* **2020**, *276*, 128213. [CrossRef]
37. Zhu, G.; Yu, X.; Xie, F.; Feng, W.J.A. Ultraviolet light assisted heterogeneous Fenton degradation of tetracycline based on polyhedral Fe_3O_4 nanoparticles with exposed high-energy {110} facets. *Appl. Surf. Sci.* **2019**, *485*, 496–505. [CrossRef]
38. Li, X.; Zeng, Z.; Zeng, G.; Wang, D.; Xiao, R.; Wang, Y.; Zhou, C.; Yi, H.; Ye, S.; Yang, Y.; et al. A "bottle-around-ship" like method synthesized yolk-shell Ag_3PO_4@ MIL-53 (Fe) Z-scheme photocatalysts for enhanced tetracycline removal. *J. Colloid Interface Sci.* **2020**, *561*, 501–511. [CrossRef]
39. Kakavandi, B.; Takdastan, A.; Jaafarzadeh, N.; Azizi, M.; Mirzaei, A.; Azari, A.J.J.; Chemistry, P.A. Application of Fe_3O_4@ C catalyzing heterogeneous UV-Fenton system for tetracycline removal with a focus on optimization by a response surface method. *J. Photochem. Photobiol. A Chem.* **2016**, *314*, 178–188. [CrossRef]

40. Hassandoost, R.; Kotb, A.; Movafagh, Z.; Esmat, M.; Guegan, R.; Endo, S.; Jevasuwan, W.; Fukata, N.; Sugahara, Y.; Khataee, A. Nanoarchitecturing bimetallic manganese cobaltite spinels for sonocatalytic degradation of oxytetracycline. *Chem. Eng. J.* **2022**, *431*, 133851. [CrossRef]
41. Loeb, S.K.; Alvarez, P.J.; Brame, J.A.; Cates, E.L.; Choi, W.; Crittenden, J.; Dionysiou, D.D.; Li, Q.; Li-Puma, G.; Quan, X. The technology horizon for photocatalytic water treatment: Sunrise or sunset? *Environ. Sci. Technol.* **2018**, *53*, 2937–2947. [CrossRef]
42. Wang, J.; Tang, J. Fe-based Fenton-like catalysts for water treatment: Catalytic mechanisms and applications. *J. Mol. Liq.* **2021**, *332*, 115755. [CrossRef]
43. Cheng, S.; Pan, X.; Zhang, C.; Lin, X.; Zhuang, Q.; Jiao, Y.; Dong, W.; Qi, X. UV-assisted ultrafast construction of robust Fe_3O_4/polydopamine/Ag Fenton-like catalysts for highly efficient micropollutant decomposition. *Sci. Total Environ.* **2022**, *810*, 151182. [CrossRef]
44. Liu, Y.; Zhao, Y.; Wang, J. Fenton/Fenton-like processes with in-situ production of hydrogen peroxide/hydroxyl radical for degradation of emerging contaminants: Advances and prospects. *J. Hazard. Mater.* **2021**, *404*, 124191. [CrossRef]
45. Zhang, D.; Yin, K.; Tang, Y.; Wei, Y.; Tang, H.; Du, Y.; Liu, H.; Chen, Y.; Liu, C. Hollow sea-urchin-shaped carbon-anchored single-atom iron as dual-functional electro-Fenton catalysts for degrading refractory thiamphenicol with fast reaction kinetics in a wide pH range. *Chem. Eng. J.* **2022**, *427*, 130996. [CrossRef]
46. Sun, Z.; Wang, S.; Chen, W. Metal single-atom catalysts for selective hydrogenation of unsaturated bonds. *J. Mater. Chem. A* **2021**, *9*, 5296–5319. [CrossRef]
47. Du, C.; Zhang, Y.; Zhang, Z.; Zhou, L.; Yu, G.; Wen, X.; Chi, T.; Wang, G.; Su, Y.; Deng, F. Fe-based metal organic frameworks (Fe-MOFs) for organic pollutants removal via photo-Fenton: A review. *Chem. Eng. J.* **2022**, *431*, 133932. [CrossRef]
48. Zhang, B.; Li, X.; Akiyama, K.; Bingham, P.A.; Kubuki, S. Elucidating the Mechanistic Origin of a Spin State-Dependent FeN x–C Catalyst toward Organic Contaminant Oxidation via Peroxymonosulfate Activation. *Environ. Sci. Technol.* **2021**, *56*, 1321–1330. [CrossRef] [PubMed]
49. Yang, T.; Yu, D.; Wang, D.; Yang, T.; Li, Z.; Wu, M.; Petru, M.; Crittenden, J. Accelerating Fe (III)/Fe (II) cycle via Fe (II) substitution for enhancing Fenton-like performance of Fe-MOFs. *Appl. Catal. B Environ.* **2021**, *286*, 119859. [CrossRef]
50. Guo, D.; Liu, Y.; Ji, H.; Wang, C.-C.; Chen, B.; Shen, C.; Li, F.; Wang, Y.; Lu, P.; Liu, W. Silicate-enhanced heterogeneous flow-through electro-Fenton system using iron oxides under nanoconfinement. *Environ. Sci. Technol.* **2021**, *55*, 4045–4053. [CrossRef]
51. Hu, Q.; Zhang, M.; Xu, L.; Wang, S.; Yang, T.; Wu, M.; Lu, W.; Li, Y.; Yu, D. Unraveling timescale-dependent Fe-MOFs crystal evolution for catalytic ozonation reactivity modulation. *J. Hazard. Mater.* **2022**, *431*, 128575. [CrossRef] [PubMed]
52. Mansouri, H.; Gholibegloo, E.; Mortezazadeh, T.; Yazdi, M.H.; Ashouri, F.; Malekzadeh, R.; Najafi, A.; Foroumadi, A.; Khoobi, M. A biocompatible theranostic nanoplatform based on magnetic gadolinium-chelated polycyclodextrin: In vitro and in vivo studies. *Carbohydr. Polym.* **2021**, *254*, 117262. [CrossRef]
53. Gholibegloo, E.; Mortezazadeh, T.; Salehian, F.; Ramazani, A.; Amanlou, M.; Khoobi, M. Improved curcumin loading, release, solubility and toxicity by tuning the molar ratio of cross-linker to β-cyclodextrin. *Carbohydr. Polym.* **2019**, *213*, 70–78. [CrossRef]
54. Gholibegloo, E.; Mortezazadeh, T.; Salehian, F.; Forootanfar, H.; Firoozpour, L.; Foroumadi, A.; Ramazani, A.; Khoobi, M. Folic acid decorated magnetic nanosponge: An efficient nanosystem for targeted curcumin delivery and magnetic resonance imaging. *J. Colloid Interface Sci.* **2019**, *556*, 128–139. [CrossRef]
55. Wu, B.; Yang, T.; Zou, D.; Jin, L.; Liang, X.; Li, T.; Huang, G.; Zhang, J. Nuclear magnetic resonance biosensor based on streptavidin–biotin system and poly-l-lysine macromolecular targeted gadolinium probe for rapid detection of Salmonella in milk. *Int. Dairy J.* **2020**, *102*, 104594. [CrossRef]
56. Jaffray, D.A. *World Congress on Medical Physics and Biomedical Engineering, 7–12 June 2015, Toronto, Canada*; Springer: Berlin/Heidelberg, Germany, 2015; Volume 51.
57. De Silva, L.; Fu, J.-Y.; Htar, T.T.; Muniyandy, S.; Kasbollah, A.; Kamal, W.H.B.W.; Chuah, L.-H. Characterization, optimization, and in vitro evaluation of Technetium-99m-labeled niosomes. *Int. J. Nanomed.* **2019**, *14*, 1101. [CrossRef] [PubMed]
58. Mortezazadeh, T.; Gholibegloo, E.; Alam, N.R.; Dehghani, S.; Haghgoo, S.; Ghanaati, H.; Khoobi, M. Gadolinium (III) oxide nanoparticles coated with folic acid-functionalized poly (β-cyclodextrin-co-pentetic acid) as a biocompatible targeted nano-contrast agent for cancer diagnostic: In vitro and in vivo studies. *Magn. Reson. Mater. Phys. Biol. Med.* **2019**, *32*, 487–500. [CrossRef] [PubMed]
59. Jenjob, R.; Kun, N.; Ghee, J.Y.; Shen, Z.; Wu, X.; Cho, S.K.; Lee, D.H.; Yang, S.-G. Enhanced conjugation stability and blood circulation time of macromolecular gadolinium-DTPA contrast agent. *Mater. Sci. Eng. C* **2016**, *61*, 659–664. [CrossRef] [PubMed]
60. Gholibegloo, E.; Ebrahimpour, A.; Mortezazadeh, T.; Sorouri, F.; Foroumadi, A.; Firoozpour, L.; Ardestani, M.S.; Khoobi, M. pH-Responsive chitosan-modified gadolinium oxide nanoparticles delivering 5-aminolevulinic acid: A dual cellular and metabolic T1-T2* contrast agent for glioblastoma brain tumors detection. *J. Mol. Liq.* **2022**, *368*, 120628. [CrossRef]
61. Thorat, N.D.; Bohara, R.A.; Yadav, H.M.; Tofail, S.A. Multi-modal MR imaging and magnetic hyperthermia study of Gd doped Fe_3O_4 nanoparticles for integrative cancer therapy. *RSC Adv.* **2016**, *6*, 94967–94975. [CrossRef]
62. Behnajady, M.; Eskandarloo, H.; Modirshahla, N.; Shokri, M. Investigation of the effect of sol–gel synthesis variables on structural and photocatalytic properties of TiO_2 nanoparticles. *Desalination* **2011**, *278*, 10–17. [CrossRef]
63. Cao, G.-J.; Jiang, X.; Zhang, H.; Croley, T.R.; Yin, J.-J. Mimicking horseradish peroxidase and oxidase using ruthenium nanomaterials. *RSC Adv.* **2017**, *7*, 52210–52217. [CrossRef]

64. Wang, L.; Liu, Y.; Lu, C.; Yang, Z.; Liu, Y.; Wang, Y.; Rao, H.; Zhang, W.; Wang, X. Ultrasonic synthesis of nano-PrO1. 8 as nanozyme for colorimetric determination of trans-resveratrol. *Sci. Rep.* **2020**, *10*, 4432. [CrossRef] [PubMed]
65. Hu, J.; Zhao, G.; Long, X.; Wang, Y.; Jiao, F. In situ topotactic fabrication of ZnS nanosheet by using ZnAl-layered double hydroxide template for enhanced tetracycline pollutant degradation activity. *Mater. Sci. Semicond. Process.* **2021**, *134*, 106007. [CrossRef]
66. Chatgilialoglu, C.; Krokidis, M.G.; Masi, A.; Barata-Vallejo, S.; Ferreri, C.; Terzidis, M.A.; Szreder, T.; Bobrowski, K. New insights into the reaction paths of hydroxyl radicals with purine moieties in DNA and double-stranded oligodeoxynucleotides. *Molecules* **2019**, *24*, 3860. [CrossRef] [PubMed]
67. Brown, P.; Gill, S.; Allen, S. Metal removal from wastewater using peat. *Water Res.* **2000**, *34*, 3907–3916. [CrossRef]
68. Vakh, C.; Malkova, K.; Syukkalova, E.; Bobrysheva, N.; Voznesenskiy, M.; Bulatov, A.; Osmolovskaya, O. Chemical and computational strategy for design of "switchable" sorbent based on hydroxyapatite nanoparticles for dispersive micro-solid phase extraction of tetracyclines. *J. Hazard. Mater.* **2021**, *419*, 126504. [CrossRef] [PubMed]
69. Ou, J.; Mei, M.; Xu, X. Magnetic adsorbent constructed from the loading of amino functionalized Fe_3O_4 on coordination complex modified polyoxometalates nanoparticle and its tetracycline adsorption removal property study. *J. Solid State Chem.* **2016**, *238*, 182–188. [CrossRef]
70. Zhu, X.; Qian, F.; Liu, Y.; Matera, D.; Wu, G.; Zhang, S.; Chen, J. Controllable synthesis of magnetic carbon composites with high porosity and strong acid resistance from hydrochar for efficient removal of organic pollutants: An overlooked influence. *Carbon* **2016**, *99*, 338–347. [CrossRef]